EUROPEAN ORGANIZATION FOR NUCLEAR RESEARCH

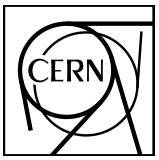

CERN-PH-EP-2021-XXX
July 2021

Study of correlated production of strangeness via the measurement of the yield ratio of $\Omega^{\pm}$ and $\phi(1020)$ with pp data of LHC run II

* Antonin Maire[1,2], Boris Hippolyte[1,2], Romain Schotter[1]
1. Université de Strasbourg, IPHC, 23 rue du Loess 67037 Strasbourg, France.
2. CNRS, UMR7178, 67037 Strasbourg, France.

ALICE analysis note

PWG-LF / PAG-Strangeness

Abstract

[Version α.1 - (git rev.3cf7e7e) - Wednesday 13th July, 2022, 00:59]

Keywords:
$\overline{\Omega}^{+}$, Ω^{-}, $\phi(1020)$,
ALICE, pp, $\sqrt{s}$ = 13 TeV (2016+2017+2018), LHC, runII, strangeness.

*by alphabetical order

[Version α.1 - (git rev.3cf7e7e) - Wednesday 13th July, 2022, 00:59]

Contents

C. Results and discussion

– Part A.

Brainstorming and considerations (for PC internal use)

I Brainstorming

I-A List of various strategical ideas

Check ID	Origin	Summary Title
Signal fit and extraction		
A.i)	Romain	Lévy-Tsallis fit to correct for signal loss at very low p_{T}
Systematic study		
B.i)	Romain	Account for correlation between selections.

Table 1: Dashboard for strategical ideas suggested by collaborators. For further details, see text with the enumerate list.

A. *Signal fit and extraction*

A.i) Perform a Lévy-Tsallis fit using the extracted signal of each p_{T}. Yields of Ω and $\phi(1020)$ would be integrated in p_{T} for all Δy bins, and not limited to a certain range.

B. *Signal fit and extraction*

B.i) Account for correlation between selections, meaning we need to extract correlation matrix.

I-B List of various checks

Check ID	Status	Origin	Summary Title
PAG Strangeness Meeting 10/08/21			
A.i)	ToDo	Jun Takahashi	Understand Ω-$\phi(1020)$ pair acceptance
A.ii)	ToDo	Jun Takahashi	Yield ratio around unity : physics message ?
A.iii)	ToDo	Roman Lietava	Understand huge discrepancy in $N_{\Omega}/N_{\mathrm{EVT}}$ per period.

Table 2: Dashboard for systematic checks anticipated or suggested by collaborators. For further details, see text with the enumerate list.

A. *PAG Strangeness Meeting 10/08/21*

A.i) Understand why Ω-$\phi(1020)$ pair acceptance so large at large Δy

A.ii) Yield ratio around unity : try to understand what is happening on the side of physics ? Idea : look p_{T} distribution of $\phi(1020)$ w/o Ω trigger

80 *A*.iii) Agree on the demand for more enriched MC production, but first, understand huge discrepancy in $N_{\Omega}/N_{\mathrm{EVT}}$ per period.

82

– Part B.

Data sets and analysis strategy

II Introduction

Colliding heavy nuclei at extremely high energy offers the possibility to form a very hot, dense and strongly interacting state of matter, called Quark Gluon Plasma (QGP). This exists for about 10^{-23} s [1], which is far shorter than the readout time of the fastest detector – the observation of such a state is therefore based on its remnants, meaning the collision products. QGP existence is associated to several signatures ; most of them have also been observed in high multiplicity proton-proton (pp) collisions, where no QGP is foreseen [2][3][4]. This questions thorougly our representation of this state of nuclear matter, and calls for a review of the concepts : either the AA collisions/QGP physics picture must be further rooted on pp collisions, or pp QCD physics must be enriched with AA considerations. One way or the other, a better description of the continuum between pp and AA collisions is needed. Nowadays, several phenomenological models are following this approach, but more experimental input are needed (Ref needed). More precisely, this input takes the shape of multi-differential measurements of identified hadrons as a function of the rapidity, the transverse momentum and the multiplicity in charged particles. This type of analysis relies on excellent particle identification capabilites, which are provided by the ALICE detector.

One of the signature usually associated to QGP is the increase of the production of strange quarks, also called strangeness enhancement. Since strangeness is very sensitive to collectivity and the enhancement of the latter is the steepest for pp collisions, this signature might be the way to shed light on the collision dynamic in small systems. Thus, a focus will be given on measurement of the correlated production of strange hadrons in pp collisions.

An example of a such measurement is proposed by Christian Bierlich : thanks to the recent developments in PYTHIA 8– namely the color rope and color shoving mechanisms – it is predicted that i) the Ω^- $[sss]$ abundancy increases when an $\phi(1020)$ $[s\bar{s}]$ is present within the event, and ii) this increase is more prominent as the gap in rapidity between the two particles reduces.

In this analysis, we propose to study the correlated production of strangeness via the measurement of the yield ratio of $(\Omega^-+\overline{\Omega}^+)$ and $\phi(1020)$ in proton-proton collisions at a center-of-mass energy $\sqrt{s} = 13$ TeV from the LHC run II, using the ALICE detector. A comparison with various Monte-Carlo (MC) generators comes to complement the results presented in this paper. For the sake of brievty, $(\Omega^-+\overline{\Omega}^+)$ will be denoted $\Omega^{\pm}$, unless otherwise stated. This paper is organized as follows. In section III, the dataset used in this analysis is presented, followed by the event selections in section IV. Further details about the analysis are showed in section V with the track and topological selections, and in section VI, systematic study is exposed. Finally, the results are given in section VII, accompanied by the comparison with phenomenological models and the discussion in section VIII.

III Data sets in pp

III-A Data sets

All pp data sets at $\sqrt{s}$ = 13 TeVcollected by ALICE during LHC run II – that is from 2016 to 2018 – are exploited in this analysis. In total, the analysis is based upon 2.2 billions minimum bias events, corresponding to an integrated luminosity of 8.12 nb^{-1} for 2016, 10.67 nb^{-1} for 2017 and 13.14 nb^{-1} for 2018 [5].

Correction in acceptance and efficiency are applied on the presented measurements. Since the yield of $\Omega^{\pm}$ is low in comparison to the one of the $\phi(1020)$, two sets of MC data are used : one general purpose for the $\phi(1020)$ and one enriched in $\Xi^{\pm}$ and $\Omega^{\pm}$. Anchored on all the periods from 2016 to 2018, the former is composed of 700 million events, while the latter consists of 12 million events, coming from only two periods (LHC17j and LHC18i). Both are generated with PYTHIA 8 using the MONASH 2013 tune and then propagated with GEANT 4. Events are reconstructed employing the same techniques and event selections as for the real data.

III-B The ALICE detector

The ALICE detector, as well as its performance, is described extensively in [6] [7]. The main sub-detectors used, in this work, are the Inner Tracking System (ITS), the Time Projection Chamber (TPC), the Time-Of-Flight detector (TOF) and the V0 detector. All are embedded inside the L3 solenoid magnet with a magnetic field of -0.5, -0.2 or +0.5 T, depending on the data taking periods [8].

The ITS consists of six cylindrical layers of silicon detectors, close to the primary vertex – positionned radially between 3.9 and 43 cm –, covering the pseudo-rapidity region $|\eta| < 0.9$. The innermost layer is composed of two layers of hydrib Silicon Pixel Detector (SPD), located respectively at 3.9 and 7.6 cm, and covers a more extended pseudo-rapidity region $|\eta| < 1.98$. The SPD is also used to reconstruct short tracks constructed from only two points, also known as tracklets. The intermediate and outermost layers are constituted separately of two layers of Silicon Drift Detector (SDD) and two layers of Silicon Strip Detector (SSD). This silicon tracker is responsible for reconstructing primary and secondary vertices.

The TPC is cylindrical gaseous detector – the gas consists of a mix of $Ne/CO_2/N_2$ for the 2016 periods, or Ar/CO_2 for 2017 and 2018 periods –, surrounding the ITS and covering the pseudo-rapidity region $|\eta| < 0.9$; its inner and outter radius are positionned respectively at 85 and 250 cm, and it has an overall length of 500 cm. The readout chambers corresponds to the two end-cap of barrel ; they are composed of multi-wire proportionnal chambers (MWPCs), arranged radially in pad rows. Thanks to its volume of 90 m^3 and its number of tracking points (up to 159), the TPC is able to reconstruct tracks of charged particle of momentum greater than 200 MeV/c, but also to provide Particle Identification (PID) informations through the measurement of their energy loss.

The TOF detector is cylindrical array of Multi-gap Resistive-Plate Chambers (MRPC), with an internal radius of 370 cm and an external one of 399 cm, which encompass the pseudo-rapidity

region $|\eta| < 0.9$. The intrisic time resolution of the MRPC is about 40 psin pp collision. The measurement of the time of flight provides PID information at intermediate momentum ($0.5 < p < 3$ GeV/c).

The V0 detector is composed of two arrays of scintillators counters, V0-A ($2.8 < \eta < 5.1$) and V0-C ($-3.7 < \eta < -1.7$), and sits respectively at 329 cm and -88 cm along the beam direction. Thanks to its excellent time resolution – 450 psfor the V0-A and 350 psfor the V0-C –, the TOF can provide trigger informations.

III-B.i Sub-Sbsection

IV Event selections and analysis strategy

IV-A Event selections

Event selection was based on a minimum bias trigger (kINT7), requiring a hit in both V0-A and V0-C counters in coincidence with the arrival of proton bunches in the two directions, which leads to the rejection of beam-gas background events. Such background events are then further removed offline, using timing information provided by the V0, and correlation between clusters and reconstructed tracklets [7]. A constrain on the longitudinal position of the reconstructed vertex ($|z| < 10$ cm, with z the position along the beam axis) is applied in order to reduce the number of unwanted collisions and ensure that reconstructed tracks are contained inside the acceptance of ALICE barrel. Only events having at least one $\Omega^{\pm}$ candidate are selected ; the set of selections for these candidates, as well as the reason for such a request, are presented in section V. For this reason, in the following, the $\Omega^{\pm}$ may be referred as the *trigger particle*.

IV-B Analysis strategy

The observable is the yield ratio of $\phi(1020)$ and $(\Omega^{-}+\overline{\Omega}^{+})$ as a function of their gap in rapidity and the multiplicity in charged particles. To get there, event analysis proceeds as follows. For each selected event, the trigger particles and the other particles of interest – namely the $\Omega^{\pm}$ and $\phi(1020)$ candidates – are reconstructed using the techniques/selections described in section V. To correlate both particles, they are associated in pairs ; invariant mass of each particle is calculated, and sorted as a function of p_{T} (of the $\Omega^{\pm}$ or $\phi(1020)$) and the rapidity difference of the pair, Δy.

After repeating these steps over all the data sample, yield of both species can be extracted from the invariant distributions, for each p_{T} and Δy bins, as presented in section V.

In order to study multiplicity dependence, the event sample is divided into multiplicity classes, based on cuts on the total charged deposited in the V0 detector (V0M amplitude) or on the number of tracklets in the region $|\eta| < 1$ ($N^{|\eta|<1}_{\mathrm{tracklets}}$) ; the V0M amplitude varies proportionnally with the number of charged particle produced in the pseudo-rapidity range of the V0 detector [9]. These classes are reported in Tab. 3, with their corresponding percentages of the total cross section INEL > 0, $\sigma/\sigma_{\mathrm{INEL>0}}$.

Multiplicity Class	I	II	III	IV	V
$\sigma/\sigma_{\mathrm{INEL>0}}$	0-0.95%	0.95-4.7%	4.7-9.5%	9.5-14%	14-19%
Multiplicity Class	VI	VII	VIII	IX	X
$\sigma/\sigma_{\mathrm{INEL>0}}$	19-28%	28-38%	38-48%	48-68%	68-100%

Table 3: Event multiplicity classes used in this analysis and their corresponding $\sigma/\sigma_{\mathrm{INEL>0}}$ [10].

V Track selections and topological selections

Measurement of primary particles are presented in this work. A primary particle corresponds to any hadron whose mean proper lifetime is larger than 1 cm, produced either directly during the collision or by the decay of particles with lifetime $c.\tau < 1$ cm originating from the interaction point [11]. Because of the short lifetime of the particles of interest – namely Ω and $\phi(1020)$–, they must be reconstructed based on their decay products. Both are reconstructed at mid-rapidity ($|y| < 0.5$), via an invariant mass analysis.

V-A Ω case

V-A.i Candidate selections

The multi-strange hadrons Ω^- and $\overline{\Omega}^+$ are studied in the following decay channel :

$\Omega^- [sss] \rightarrow \Lambda [uds]\ \mathrm{K}^-[\bar{d}\bar{s}]$ B.R. 67.8 %
$\overline{\Omega}^+ [\bar{s}\bar{s}\bar{s}] \rightarrow \overline{\Lambda} [\bar{u}\bar{d}\bar{s}]\ \mathrm{K}^+[u\bar{s}]$ B.R. 67.8 %

$\Lambda [uds] \rightarrow \mathrm{p}[uud]\ \pi^-[\bar{u}d]$ B.R. 63.9 %
$\overline{\Lambda} [\bar{u}\bar{d}\bar{s}] \rightarrow \overline{\mathrm{p}}[\bar{u}\bar{u}\bar{d}]\ \pi^+[u\bar{d}]$ B.R. 63.9 %

The Λ and Ω being hyperons, they follow a V-shaped decay topology, typical of this family of particles. The multi-strange hadron decay into a kaon and a Λ. The latter being electrically neutral, only the charged meson is detected at this stage ; the meson is considered as a bachelor particle. Further away, the baryon daughter decays into two oppositely charged particles (V^0 decay) : a proton and a pion. Depending on their electric signs, one is called positive and the other negative. Thus, the Ω undergoes two step decay process, known as cascade decay. In the following, the usage of the term *cascade* can refer to Ω, and similarly the term *V0* to Λ.

Cascade reconstruction is done by associating three tracks ; these tracks must first pass a set of selections. Only the associations matching the topological selections are considered. The selections used in this work are summarised in Tab. 4.

Only tracks with at least 70 crossed rows in the TPC out of 159 are retained in the analysis. Each decay products must be contained inside the fiducial tracking volume, $|\eta| < 0.8$. All the tracks must have been refitted, with the Kalman filter in the TPC, backwards to the primary vertex. The energy loss (dE/dx) of all decay products is requested to be compatible in $\pm$ 3 σ with the considered PID hypothesis. Tracks exhibiting a kink topology are discarded.

Cascade candidates are required to be in the rapidity window $|y| < 0.5$. Ω candidates whose reconstructed mass under Ξ hypothesis lies within a window of $\pm$ 8 MeV/c^2around the Ξ PDG mass are rejected. A similar selection is also applied on the V0 ; only V0 candidates compatible with the Λ PDG mass within $\pm$ 8 MeV/$c^2$are selected. A set of topological selections are used in order to identify V0 and cascade decay topologies.

Topological variable	Selections Ω^- ($\overline{\Omega}^+$)
V0	
V0 radius (cm)	> 1.1
V0 CosPA	> 0.97
$\lvert m(V0)$ - $m_{\mathrm{PDG}}(\Lambda)\rvert$ (GeV/c^2)	< 0.008
DCA pos. to prim. vtx (cm)	> 0.03(0.04)
DCA neg. to prim. vtx (cm)	> 0.04(0.03)
DCA V0 to prim. vtx (cm)	> 0.06
DCA between V0 daughters (std dev)	< 1.5
Cascade	
Casc. radius (cm)	> 0.5
Casc. Lifetime (cm)	$< 3 \times 2.461$
DCA bach. to prim. vtx (cm)	> 0.04
DCA between the casc. daughters (std dev)	< 1.3
Casc. CosPA	> 0.999
Bach-baryon PA	> 0.04
Track variable	Selections Ω^- ($\overline{\Omega}^+$)
Daughter pseudo-rapidity interval	$\lvert\eta\rvert < 0.8$
TPC refit	✔
Kink Topology	✗
Nbr of crossed rows	> 70
TPC dE/dx	$< 3\,\sigma$
Candidate variable	Selections Ω^- ($\overline{\Omega}^+$)
Cascade p_{T} interval (GeV/c)	$1 < p_{\mathrm{T}} < 5$
Cascade rapidity interval	$\lvert y\rvert < 0.5$
$\lvert m$(hyp. $\Xi^{\pm}$) - $m_{\mathrm{PDG}}(\Xi)\rvert$ (GeV/c^2)	> 0.008
MC association (MC only)	Correct identity assumption on casc. and daughters

Table 4: Summary of the topological selections and track selections used for the reconstruction of $\Omega^{\pm}$.

V-A.ii Raw signal extraction

The signal extraction is performed as a function of p_{T}. A fit is performed using a modified gaussian for the signal and a first order polynomial for the background (Ref formula modified gaussian). This allows to extract the mean value (μ) and the width of the gaussian(σ). Signal region is defined in $\mu \pm 5\sigma$; background region corresponds to bands, of the same width, surrounding on both side the signal area, that is $]\mu - 10\sigma; \mu - 5\sigma] \cup [\mu + 5\sigma; \mu + 10\sigma[$. The raw

signal is then extracted from the integral of the modified gaussian within the signal region.

$$\frac{\mathrm{d}N}{\mathrm{d}m_{\Lambda K}} = A \cdot \exp[-0.5 \cdot x^{(1+\frac{1}{1+0.5\cdot x})}],\ x = \left|\frac{m_{\Lambda K} - \mu}{\sigma}\right| \tag{1}$$

An example of an invariant mass distribution can be found in Fig. 1. A peak of over-population emerges around the PDG mass of the Ω, and one may notice that purity exceeds the 90%. Such a pure sample has been obtained by restricting the range of possible value on the cosine of pointing angle of the cascade daughters ; this tight selection value corresponds to the one displayed in Tab. 4.

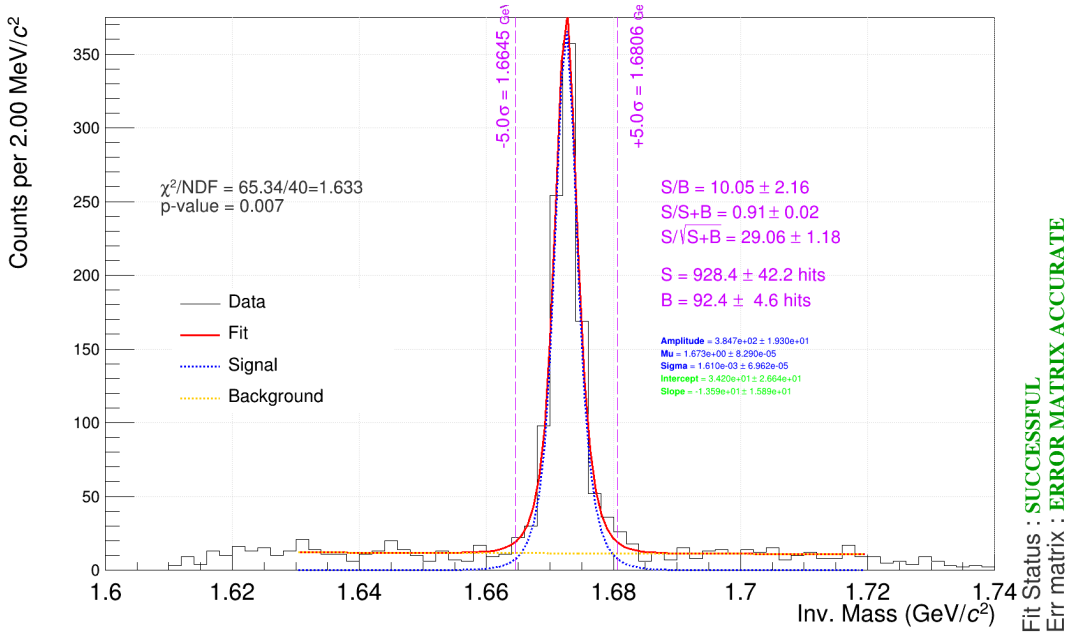

Fig. 1: Invariant mass distribution for Ω in multiplicity class I. The candidates are reconstructed in $|y| < 0.5$. Blue dashed line represents the signal fit ; the region delimited by the two dashed purple lines defines the *signal region*, used to extract raw signal of Ω.

V-B $\phi(1020)$ case

V-B.i Candidate selections

$\phi(1020)$ resonances are studied in the following decay channel :

$\phi(1020)$ $[s\bar{s}] \rightarrow \mathrm{K}^+[u\bar{s}]\ \mathrm{K}^-[\bar{u}s]$ B.R. 49.2 %

This resonance is reconstructed by forming pairs of tracks of opposite charge ; in the following, these pairs will be called "same-event pairs" . Due its short lifetime of 46.4 fm[12], misassociations can not be discarded with a set of geometrical selections like in Ω reconstruction, leading

a large combinatorial background. This background is evaluated and then substracted using two techniques presented later in this section.

Tracks are being selected using standard ITS/TPC track cuts from 2011. High-quality tracks are ensured by restricting the number of crossed rows in TPC to be greater 70 (out of 159 pad rows) ; its ratio to the number of findable clusters should exceed 0.8. This is also achieved via cuts on χ^2 per cluster. The latter quantity on reconstructed tracks in the TPC and in the ITS are requiered to be smaller than 4 and 36 respectively ; χ^2 value between TPC track constrained to the SPD vertex and global track must be inferior to 36. Only tracks following this requierements are retained : at least one hit in the innermost layer of the ITS, and the distance of closest approach to the primary vertex (DCA) lower than $0.0105+0.035p_{\mathrm{T}}^{-1.01}$ cm in the transverse plane and 2 cm along the longitudinal direction. In addition, kink decay topologies are discarded. This allows to reject secondary particles coming from weak decay. Each track has to lie in the pseudo-rapidity window $|\eta| < 0.5$ and to carry a transverse momentum between 0.15 and 4 GeV/c. Energy loss in the TPC must be consistent with the PID hypothesis within ± 2 σ. If track matches a hit in the TOF, time of flight measurement is then used to select tracks compatible in ± 3 σ with particle's species hypothesis. Only resonance candidates sitting in the rapidity interval $|y| < 0.5$ are selected.

To tackle the combinatorial background, two approaches have been followed in this work. In the "mixed-events" method, each track from one event is paired with tracks of opposite charge coming from five different events in order to build uncorrelated pairs. Only the events whose difference in longitudinal position of primary vertex remains in ± 1 cm and multiplicity percentile, calculated from the V0M amplitude, coincides with ± 10% are considered for the mixing. The mixed-event distribution is normalized by two times the number of mixed-events. In the second approach, one track from the resonance candidate (either the positive or the negative daughter) is rotated by 180 degree along the z axis. Doing so, correlation between the two daughters is broken, leading to an uncorrelated pair. In this case, normalization factor is calculated such that the integral of the same-event and rotated-event distribution in the region $1.04 < m_{KK} < 1.06$ GeV/c^2coincides.

After normalization, the final invariant mass distribution is obtained by substraction of the same-event pair distribution by the uncorrelated pair distribution. In the following, the remaining background will be named *residual background*.

V-B.ii Raw signal extraction

For each p_{T} bin, in the mass window $0.990 < m_{KK} < 1.060$ GeV/c^2, signal peak is fitted by a Voigt function (convolution of Breit-Wigner, for the ideal signal, and a Gaussian, for detector resolution) added by a first order polynomial for the residual background. Raw signal is then extracted by the integral of the Voigt function within the fitting range.

$$\frac{\mathrm{d}N}{\mathrm{d}m_{KK}} = \frac{A\Gamma}{(2\pi)^{3/2}\sigma}\int_{-\infty}^{\infty}\exp\Big[-\frac{(m_{KK}-m')^2}{2\sigma^2}\Big]\frac{1}{(m'-\mu)^2+\Gamma^2/4}\mathrm{d}m' \tag{2}$$

Track variable	Selections $\phi(1020)$
p_T interval (GeV/c)	$0.15 < p_T < 4$
Daughter pseudo-rapidity interval	$\|\eta\| < 0.8$
TPC dE/dx	$< 2\ \sigma$
TOF β (veto only)	$< 3\ \sigma$
Standard ITS/TPC Cuts 2011	
ITS refit	✔
TPC refit	✔
Kink Topology	✗
Nbr of crossed rows	> 70
Nbr of crossed rows over findable clusters	≥ 0.8
χ^2_{TPC}	< 4
$\chi^2_{\text{TPC-CG}}$	< 36
χ^2_{ITS}	< 36
Nbr of clusters in SPD	≥ 1
DCAxy (cm)	$< 0.0105 + 0.035\ p_T{}^{-1.01}$
DCAz (cm)	< 2
DCAToVertex2D	✗
RequireSigmaToVertex	✗
Candidate variable	Selections $\phi(1020)$
Resonance rapidity interval	$\|y\| < 0.5$
MC association (MC only)	Correct identity assumption on casc. and daughters

Table 5: Summary of the track and candidate selections used for the reconstruction of $\phi(1020)$.

Width of the $\phi(1020)$ is fixed to its nominal value $\Gamma = 4.29$ MeV[12], and the resolution σ is kept as a free parameter. Fig. 2 illustrates an example of the invariant mass distribution obtained with the aforementionned procedure, on which a $\phi(1020)$ peak arises on top of a residual background.

V-C Yield extraction

For each p_T bin, raw yield is calculated from the previously extracted raw signal using the expression Eq. V-C :

$$\left.\frac{\mathrm{d}^2N}{\mathrm{d}p_T\mathrm{d}y}\right|_{\text{RAW}} = \frac{S_{\text{raw}}}{\Delta p_T \Delta y} \tag{3}$$

Raw particle yields are then corrected in acceptance (A) and efficiency (ε_{REC}) using a MC data sample : the enriched one for the Ω, and the general purpose one for the $\phi(1020)$. The goal is to estimate the efficiency factor, ε, in Eq. V-C. The numerator corresponds to the number of reconstructed $\Omega/\phi(1020)$; reconstruction is performed as if it would be real data, with an addi-

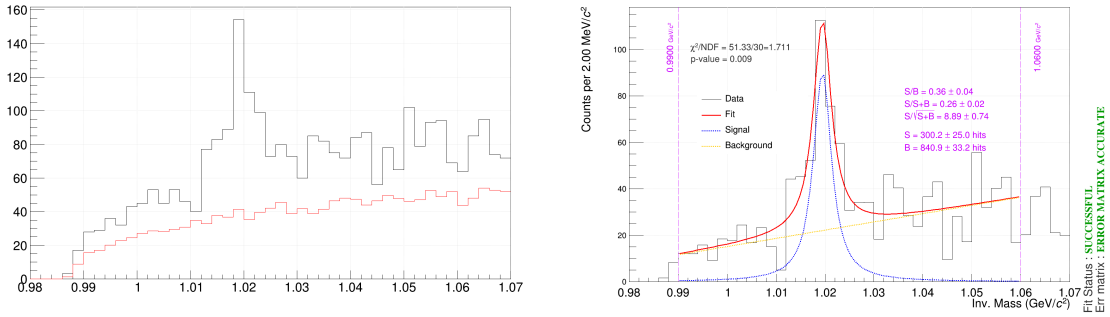

(a) (b)

Fig. 2: Invariant mass distributions for $\phi(1020)$ in multiplicity class I. The candidates are reconstructed in $|y| < 0.5$. Fig. 2a : Same-event pairs distribution in black, normalized mixed-event pairs distribution in red. Fig. 2 : Substraction of same-event and normalized mixed-pair distributions. Blue dashed line represents the signal fit ; the region delimited by the two dashed purple lines defines the *signal region*, used to extract raw signal of $\phi(1020)$.

tionnal request : only reconstructed cascade/resonance associated to a generated Ω/rmPhiMes are selected. This ensures the efficiency factor to be defined between 0 and 1. Denominator contains the number of generated particles in the selected events, coming directly from MC truth. To avoid bin flow effect, the same set of selection must be applied on both numerator and denominator ; this concerns the cuts on the rapidity and on the transverse momentum. Fig. 3a and 3b show efficiency factors as a function of p_{T}, for Ω and $\phi(1020)$ respectively.

$$\varepsilon = A \times \varepsilon_{\mathrm{REC}} \times \mathrm{B.R.} = \frac{\text{Number of reconstructed } h^{\pm}}{\text{Number of generated } h^{\pm}} \tag{4}$$

Once efficiency factors are evaluated for each p_{T} bin, corrected yields is given by $\mathrm{dN/dptdy}|_{\mathrm{RAW}}/\varepsilon$. Uncertainties on ε are not propagated, they will be included in the systematic uncertainties. Once the yield is extracted for each p_{T} bin, they are all summed and uncertainties are added in quadrature.

Following the prediction to be tested, only events presenting at least one $\phi(1020)$ resonance should be selected, and Ω yield should be extracted afterwards. As a matter of fact, it is completely equivalent to do the opposite, meaning : filter events with at least one Ω, and then extract $\phi(1020)$ yield. However, it has been shown, in sections V-A and V-B, that both species have distinct purities. Consequently, even if the two approaches of the PYTHIA 8 prediction are equivalent, one may introduce more noise than the other. With a purity exceeding 90%, the second approach appears to be the most strategic choice.

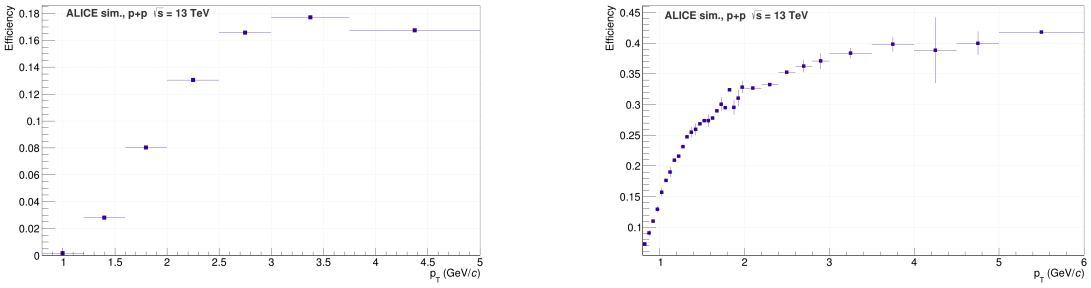

(a) (b)

Fig. 3: Efficiency factors as a function of p_{T} for 3a) Ω and 3b) $\phi(1020)$. Efficiency factor is integrated in multiplicity of the event and in rapidity of the candidates. The candidates are reconstructed in $|y| < 0.5$. Fig. 3a has been obtained with the MC sample enriched in $\Xi^-+\overline{\Xi}^+$ and $\Omega^-+\overline{\Omega}^+$; Fig. 3b has been extracted using five runs of the general purpose MC.

VI Systematic studies

Several sources of systematic uncertainties are considered in this study ; they will be detailed and quantified separately for both particles. Uncertainties related to the observable of interest are also addressed.

VI-A Ω case

Concerning the cascade, the main source of systematic uncertainties are the following : track and topological selections, signal extraction, and material budget.

VI-A.i Track and topological selections

VI-A.ii Signal extraction

VI-A.iii Material budget

VI-B $\phi(1020)$ case

Multiple source of systematic uncertainties are considered for resonances : track and pair selections, signal extraction, combinatorial background, material budget.

VI-B.i Track and pair selections

VI-B.ii Signal extraction

VI-B.iii Combinatorial background

VI-B.iv Material budget

VI-C Yield ratio

VI-C.i Combinatorial background

Topological variable	Very loose	Loose	Default	Tight	Very Tight
V0					
V0 radius (cm)			> 1.1		
V0 CosPA	> 0.95	> 0.96	> 0.97	> 0.98	> 0.99
$\lvert m(V0) - m_{\mathrm{PDG}}(\Lambda)\rvert$ (GeV/c^2)	< 0.010	< 0.009	< 0.008	< 0.007	< 0.006
DCA pos. to prim. vtx (cm)			> 0.03(0.04)		
DCA neg. to prim. vtx (cm)			> 0.04(0.03)		
DCA V0 to prim. vtx (cm)			> 0.06		
DCA V0 daughters (std dev)	< 2.5	< 2	< 1.5	< 1	< 0.5
Cascade					
Casc. radius (cm)			> 0.5		
Casc. Lifetime (cm)			< 3 × 2.461		
DCA bach. to prim. vtx (cm)			> 0.04		
DCA casc. daughters (std dev)	< 2	< 1.5	< 1.3	< 1	< 0.5
Casc. CosPA			> 0.999		
Bach-baryon PA			> 0.04		
Track variable	Very loose	Loose	Default	Tight	Very Tight
Daughter pseudo-rapidity interval			$\lvert\eta\rvert$ < 0.8		
TPC refit			✔		
Kink Topology			✗		
Nbr of crossed rows	> 60	> 65	> 70	> 80	> 90
TPC dE/dx	< 4 σ	< 3.5 σ	< 3 σ	< 2.5 σ	< 2 σ
Candidate variable	Very loose	Loose	Default	Tight	Very Tight
Cascade p_{T} interval (GeV/c)			1 < p_{T} < 5		
Cascade rapidity interval			$\lvert y\rvert$ < 0.5		
$\lvert m$(hyp. $\Xi^{\pm}$) - $m_{\mathrm{PDG}}(\Xi)\rvert$ (GeV/c^2)			> 0.008		
MC association (MC only)			Correct identity assumption on casc. and daughters		

Table 6: Summary of the systematic variations of topological and track selections of Ω^- and $\overline{\Omega}^+$ in parenthesis.

– Part C.

Results and discussion

VII Results

VII-A Experimental results

VII-A.i Sub-Sbsection

The yield ratio distribution of $\phi(1020)$ and $\Omega^{\pm}$, measured at $|y| < 0.5$, is shown in Fig. 4a for the multiplicity class I. One may notice the arising of a peak around Δy close to zero ; this suggests an increase of $\phi(1020)$ yield, as it gets closer to the $\Omega^{\pm}$.

Nevertheless, as explained in section IV, all the $\phi(1020)$ within the event are paired with the trigger particle, meaning that associations of uncorrelated particles are present in Fig. 4a. Instead, one can look at the yield ratio distribution of $\phi(1020)$ and $\Omega^{\pm}$ with respect to the very same ratio but formed with uncorrelated pairs. The latter is obtained using an event-mixing technique, which consists in pairing $\Omega^{\pm}$ from one event with $\phi(1020)$ from five different events. Those events must pass the following criteria : the difference in longitudinal position of the primary vertex has to remain within ± 1 cm, and they are requiered to share the same multiplicity percentile with a tolerance of ± 10 %. Yield ratio distribution of $\phi(1020)$ and $\Omega^{\pm}$, based upon uncorrelated pairs, is depicted on Fig. 4b.

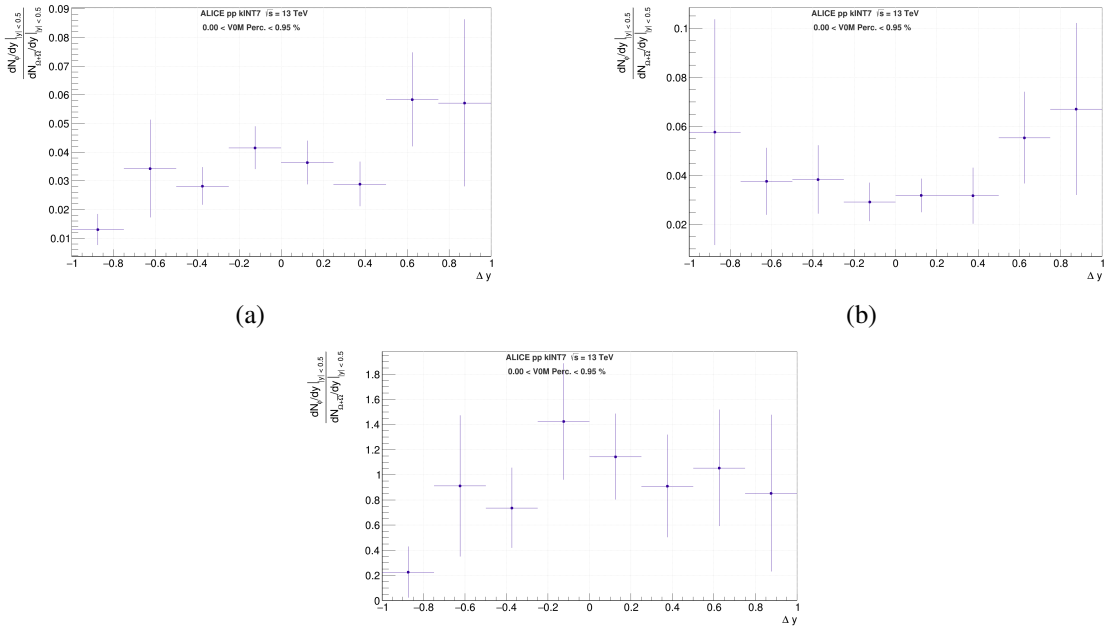

(a) (b)

(c)

Fig. 4: Yield ratio of $\phi(1020)$ and $(\Omega^{-}+\overline{\Omega}^{+})$, event-by-event, as a function of their difference in rapidity, Δy. Fig. 4a depicts the efficiency corrected yield ratio with same-event pairs ; both species are corrected individually. Fig. 4b represents the efficiency corrected yield ratio with mixed-event pairs. Division of the two previous yield ratio is presented in Fig. 4c, meaning the efficiency and pair acceptance corrected yield ratio.

$\phi(1020)$-$\Omega^{\pm}$ pair acceptance and efficiency corrected yield distribution, measured at $|y| < 0.5$, is presented on Fig. 4c for class I events. A trend seems to emerge : the yield ratio increases as the $\phi(1020)$ gets closer to the $\Omega^{\pm}$. Yet, this production enhancement is comprised within the error bars. It is interesting to note that the ratio is distributed around unity, meaning that the yield of $\phi(1020)$ is almost equal to the one of Ω, whenever Ω is present within the event.

VII-B Comparison with MC models

VIII Discussion

VIII-A SbSection

VIII-A.i Sub-Sbsection

Acknowledgements

For Romain Schotter, this work of the Interdisciplinary Thematic Institute QMat, as part of the ITI 2021 2028 program of the University of Strasbourg, CNRS and Inserm, has been supported by IdEx Unistra (ANR 10 IDEX 0002), and by SFRI STRAT'US project (ANR 20 SFRI 0012) and EUR QMAT ANR-17-EURE-0024 under the framework of the French Investments for the Future Program.

References

[1] J. D. Bjorken, *Highly relativistic nucleus-nucleus collisions: The central rapidity region*, *Physical Review D* **27** (Jan., 1983) 140–151. Publisher: American Physical Society. /link.aps.org/doi/10.1103/PhysRevD.27.140, DOI Link.

[2] CMS Collaboration, *Evidence for collective multi-particle correlations in pPb collisions*, *Physical Review Letters* **115** (June, 2015) 012301. arXiv: 1502.05382. arxiv.org/abs/1502.05382, DOI Link.

[3] ALICE Collaboration, *Enhanced production of multi-strange hadrons in high-multiplicity proton-proton collisions*, *Nature Physics* **13** (June, 2017) 535–539. arXiv: 1606.07424. arxiv.org/abs/1606.07424, DOI Link.

[4] ALICE Collaboration, *Multiplicity and transverse momentum evolution of charge-dependent correlations in pp, p-Pb, and Pb-Pb collisions at the LHC*, *The European Physical Journal C* **76** (Feb., 2016) 86. arXiv: 1509.07255. arxiv.org/abs/1509.07255, DOI Link.

[5] ALICE Collaboration, *ALICE 2016-2017-2018 luminosity determination for pp collisions at $\sqrt{s}$ = 13 TeV*, .

[6] The ALICE Collaboration et al., *The ALICE experiment at the CERN LHC*, *Journal of Instrumentation* **3** (Aug., 2008) S08002–S08002. Publisher: IOP Publishing. /doi.org/10.1088/1748-0221/3/08/s08002, DOI Link.

[7] ALICE Collaboration, *Performance of the ALICE Experiment at the CERN LHC*, *International Journal of Modern Physics A* **29** (Sept., 2014) 1430044. arXiv: 1402.4476. arxiv.org/abs/1402.4476, DOI Link.

[8] *AliDPGReconstructedDataTakingPeriodspp13TeV < ALICE < TWiki*, . /twiki.cern.ch/twiki/bin/view/ALICE/AliDPGReconstructedDataTakingPeriodspp13TeV.

[9] ALICE Collaboration, *Performance of the ALICE VZERO system*, *Journal of Instrumentation* **8** (Oct., 2013) P10016–P10016. arXiv: 1306.3130. arxiv.org/abs/1306.3130, DOI Link.

[10] ALICE Collaboration, *Production of light-flavor hadrons in pp collisions at $\sqrt{s}$ = 7 and $\sqrt{s}$ = 13 TeV*, *arXiv:2005.11120 [hep-ex, physics:nucl-ex]* (May, 2020). arXiv: 2005.11120. arxiv.org/abs/2005.11120.

[11] *The ALICE definition of primary particles*, Number: ALICE-PUBLIC-2017-005, June 2017. /cds.cern.ch/record/2270008.

[12] *pdgLive*, . pdglive.lbl.gov/Viewer.action.

The ALICE Collaboration